ARTICLES

Decomposition of Anthranil. Single Pulse Shock-Tube Experiments, Potential Energy Surfaces and Multiwell Transition-State Calculations. The Role of Intersystem Crossing†

Assa Lifshitz,* Carmen Tamburu, Aya Suslensky, and Faina Dubnikova

Department of Physical Chemistry, The Hebrew University, Jerusalem 91904, Israel

Received: November 3, 2005; In Final Form: January 11, 2006

The thermal decomposition of anthranil diluted in argon was studied behind reflected shock waves in a 2 in. i.d. pressurized driver single-pulse shock tube over the temperature range 825−1000 K and overall densities of $\sim 3 \times 10^{-5}$ mol/cm^3. Two major products: aniline and cyclopentadiene carbonitrile (accompanied by carbon monoxide) and four minor products resulting from the decomposition were found in the postshock samples. They were, in order of decreasing abundance, pyridine, CH_2═CHCN, HCN and CH≡C−CN, and comprised only a few percents of the overall product distribution. Quantum chemical calculations were carried out to determine the sequence of the unimolecular reactions that lead to the formation of cyclopentadiene carbonitrile and of phenylnitrene/phenylimine that are the precursors of aniline. They form aniline by reactions with traces of water impurities. To produce cyclopentadiene carbonitrile, two main processes must take place: CO elimination and ring contraction from a six- to a five-membered ring. It was shown that this can occur via two parallel pathways where CO elimination takes place prior to or following ring contraction. Singlet potential energy surfaces for all the elementary reactions that lead to the formation of cyclopentadiene carbonitrile and phenylnitrene/phenylimine were obtained. Their rate constants were calculated on the basis of the results of the quantum chemical calculations using transition-state theory. A kinetic scheme containing these reactions was constructed and multiwell calculations were performed to evaluate the mole percent of the products as a function of temperature. A very serious disagreement between the experimental results and the results of calculations showed that the singlet PESs could not account for the observed experimental rates. No other singlet PESs that lead to the formation of these products could be found. In view of this observation, attempts to find pathways that lead to the formation of cyclopentadiene carbonitrile and phenylnitrene/phenylimine on triplet surfaces were made. Such surfaces were found, and singlet ↔ triplet intersystem crossing probabilities and crossing rate constants were calculated as well as the rate constants of all the elementary steps on the triplet surfaces. A reaction scheme was constructed and multiwell calculations were performed, including also the pathways on the singlet surfaces, to evaluate the mole percent of the products as a function of temperature. The agreement between the experimental results and these calculations was quite satisfactory.

I. Introduction

Anthranil (2,1-bezisoxazole) is one of three isomers of a molecule where a five-membered ring containing both nitrogen and oxygen are fused to benzene.

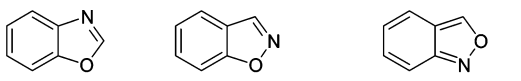

benzoxazole 1,2-benzisoxazole 2,1-benzisoxazole (anthranil)

Benzoxazole, having no weak N−O bond, is the most stable isomer. 2,1-benzisoxazole is the most unstable having a weak N−O bond, on one hand, and no resonance stabilization in the six-membered ring, on the other hand. The heats of formation of the three isomers are thus 10.8 (benzoxazole),[1] 33.3 (1,2-benzisoxazole)[2] and 41.2 kcal/mol (2,1-benzisoxazole)[2] at 298.15 K, respectively. On the basis of the relative stability of these three isomers, it is expected that the thermal decomposition of 2,1-benzisoxazole, which is the subject of this investigation, will proceed at the lowest temperatures in comparison to the other two. It is expected also that the initiation reaction in both 1,2- and 2,1-benzisoxazole will be the rupture of the weak N−O bond, as has been shown in the decomposition of isoxazole[3] and 5-methylisoxazole[4] and the isomerization of 3,5-dimethyl-isoxazole.[5]

Whereas a large number of catalytic reactions of anthranil and it derivatives have been reported in the literature,[6] we are not aware of many studies that deal with the homogeneous reactions of anthranil. Tsang et al.[7] have reported on the formation of anthranil in the pyrolysis of *o*-nitrotoluene and its

† Part of the "Chava Lifshitz Memorial Issue".

* Corresponding author. E-mail: Assa@vms.huji.ac.il.

10.1021/jp056339v CCC: $33.50
Published on Web 02/23/2006

subsequent decomposition. They have suggested possible mechanisms for the formation of anthranil from *o*-nitrotoluene and for the production of cyclopentadiene carbonitrile and phenylnitrene due to its decomposition. They did not give, however, any details on the rates of the various steps that lead to the final products, they have only reported on the rate of the overall decomposition of anthranil. We are not aware also of any quantum chemical calculations that verify the interpretation of the experimental results.

The formation of phenylnitrene and cyclopentadiene carbonitrile from five-membered rings fused to benzene has also been reported in the literature, for example, in the pyrolysis of 1*H*-benzotriazole.[8−10] Here nitrogen is eliminated rather than CO and in addition to cyclopentadiene carbonitrile the formation of aniline and of azobenzene has also been reported.

In this investigation experimental results and detailed quantum chemical calculations on the decomposition of anthranil are reported. It will be shown that singlet potential energy surfaces could not account for the formation rate of the main products of the decomposition, whereas mole percents calculated on triplet potential energy surfaces agreed quite well with the experimental observations.

II. Experimental Section

1. Shock Tube, Materials and Analysis. The thermal decomposition of anthranil was studied behind reflected shock waves in a 2 in. i.d. single pulse shock tube. The driven section was 4 m long, and the driver had a variable length up to a maximum of 2.7 m and could be varied in small steps to tune for the best cooling conditions. A 36 L dump tank was connected to the driven section near the diaphragm holder to quench transmitted shocks. The tube, the gas handling system, the reaction mixture bulbs and the transfer tubes were all maintained at 130 °C with an accuracy of ±2 °C. The shock tube and the mode of its operation were described in the past.[11]

Reflected shock temperatures were determined from the extent of decomposition of secondary chloropropane: $(CH_3)_2CHCl \rightarrow C_3H_6 + HCl$. This is a first-order unimolecular reaction that under the temperature and pressure conditions of this investigation has a rate constant of $k_{first} = 3.24 \times 10^{13} \exp(-50.52 \times 10^3/RT)\ s^{-1}$, where R is expressed in units of cal/(K mol).[12] The relation

$$T = -(E/R)/\left[\ln\left\{-\frac{1}{At}\ln(1-\chi)\right\}\right]$$

was used, where t is the reaction dwell time, approximately 2 ms, A and E are the Arrhenius parameters of the standard reaction and χ is the extent of decomposition defined as $\chi = [C_3H_6]_t/([C_3H_6]_t + [(CH_3)_2CHCl]_t)$. Density ratios were calculated from the measured incident shock velocities using the three conservation equations and the ideal gas equation of state. Cooling rates were approximately 5×10^5 K/s.

After pumping down a 12 L glass bulb to $\sim 10^{-5}$ Torr, an amount of liquid corresponding to 0.5% anthranil was injected into the evacuated bulb that was then filled to 1 atm with argon containing 0.08% of the internal standard, $(CH_3)_2CHCl$. The bulb served as storage for the reaction mixture.

Three gas chromatographic analyses for each postshock mixture provided the product distribution and the temperature. A flame ionization detector (FID) with a 2 m Porapak N column was used to determine the ratio $[C_3H_6]/([C_3H_6] + [(CH_3)_2CHCl])$ for the temperature calculation. A nitrogen phosphorus detector (NPD) with a 2 m temperature programmed Porapak N column was used to determine the low molecular weight fragmentation products, and a GC−MS with a 2 m temperature programmed Tenax column was used to determine the concentrations of aniline, cyclopentadienecarbonitrile and anthranil. Carbon monoxide was evaluated from nitrogen−oxygen mass balance considerations assuming that there was a minimal loss of material if at all. A typical chromatogram showing traces obtained on the three detectors is given in Figure 1.

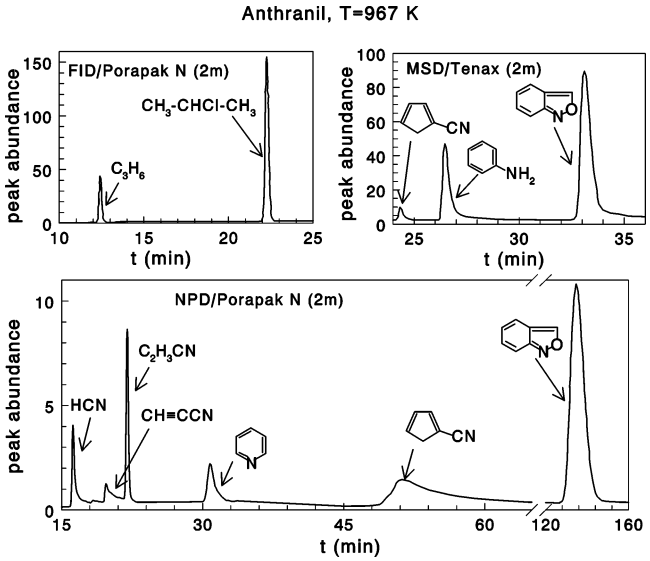

Figure 1. Gas chromatogram showing the products of anthranil decomposition. Top left: $(CH_3)_2CHCl$ and C_3H_6 from the ratio of which the temperature behind the reflected shock is calculated. Top right: MSD spectrum of anthranil and the main decomposition products. Bottom: NPD spectrum of the fragmentation products. (Aniline could not be detected on the Porapak N column.)

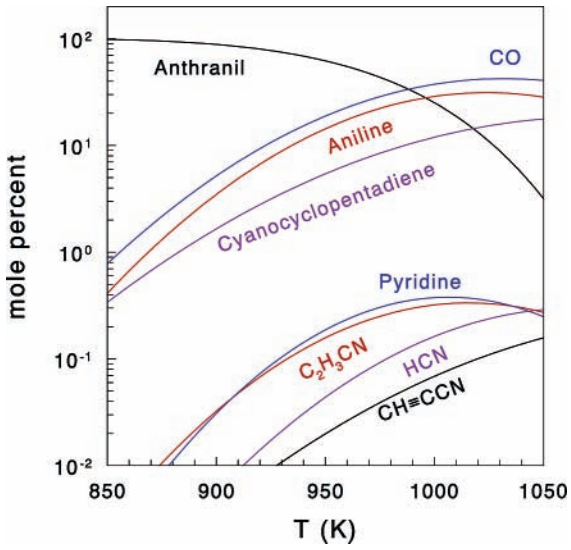

Figure 2. General distribution of the reaction products in the decomposition of anthranil.

2. Experimental Results. To determine the distribution of reaction products, some 80 tests were run, covering the temperature range 825−1050 K. Figure 2 shows the general product distribution over the entire temperature range including carbon monoxide. As can be seen, aniline, cyclopentadiene carbonitrile and carbon monoxide (that is formed together with these two products) are of the highest concentrations and the four fragmentation products: pyridine, acrylonitrile, hydrogen cyanide and cyanoacetylene, have considerably lower concentrations. Figure 3 shows the experimental mole percent for each one of the products; carbon monoxide is not included. It should

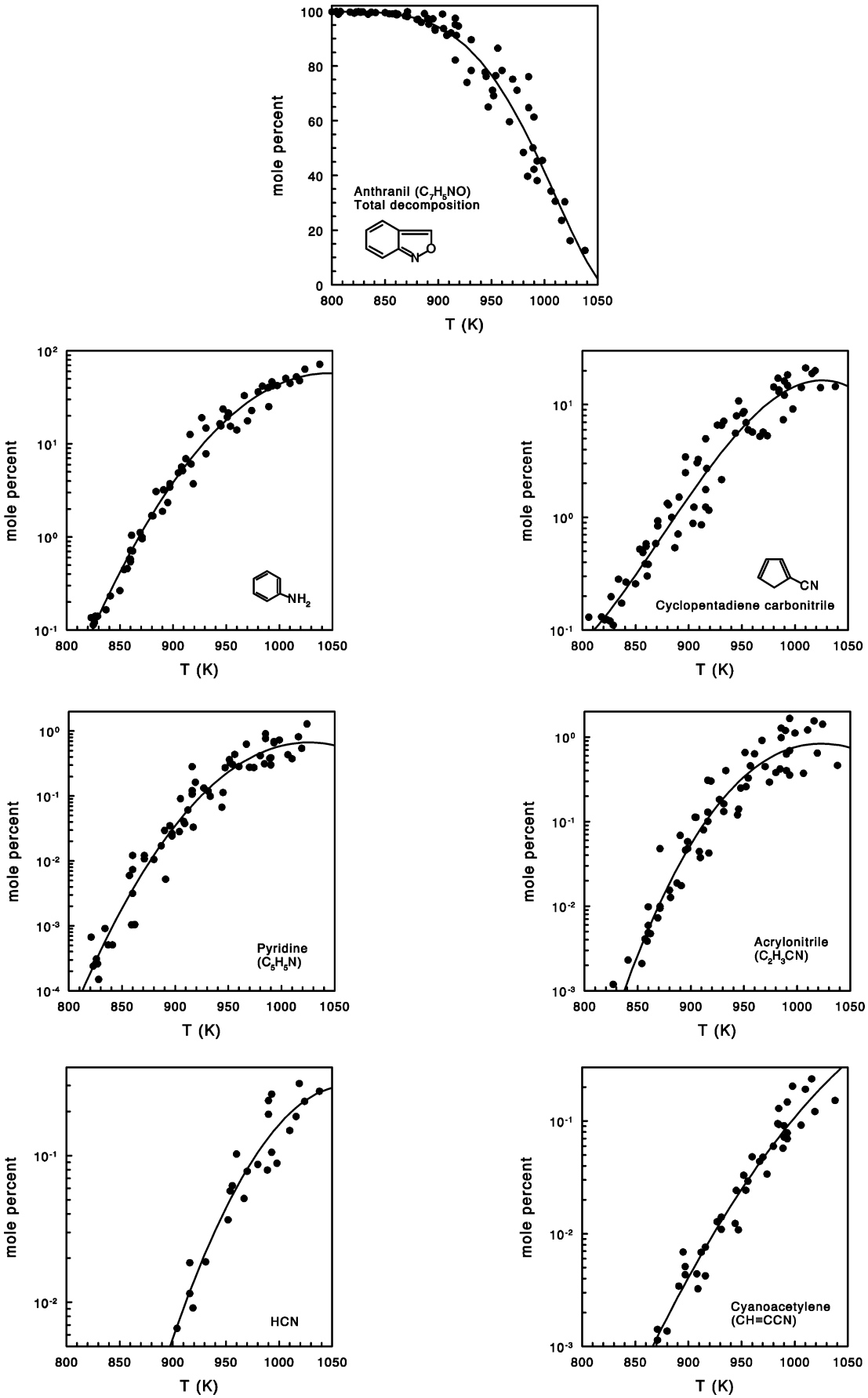

Figure 3. Detailed distribution of the reaction products in the decomposition of anthranil, carbon monoxide not included.

be stressed again that aniline is not a direct product of anthranil decomposition. It is obtained from the intermediates C_6H_5-N: (or $C_6H_4^{\bullet}-NH^{\bullet}$) that are formed in the process and that find a way to add two hydrogen atoms probably from traces of water

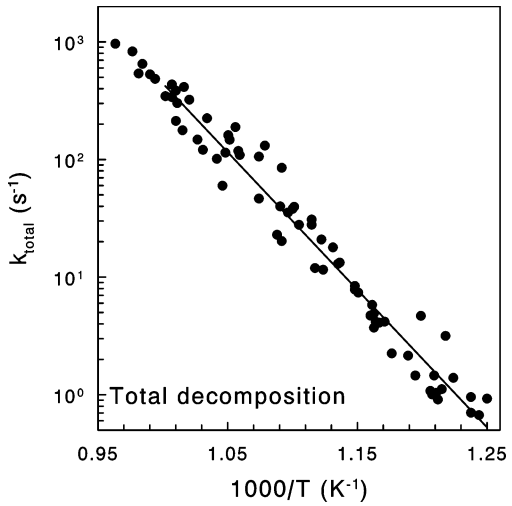

Figure 4. Arrhenius plot for the total decomposition of anthranil. $k_{total} = 2.24 \times 10^{14} \exp(-53.5 \times 10^3/RT)\ s^{-1}$, where R is expressed in units of cal/(K mol).

that are absorbed on the walls of the injection system of the GC, or in the column or elsewhere.

Figure 4 shows the rate constant for the overall decompositions of anthranil, calculated as a first-order rate constant from the relation: $k_{total} = -\ln\{[anthranil]_t/[anthranil]_0\}/t$. The value obtained is $k_{total} = 2.24 \times 10^{14} \exp(-53.5 \times 10^3/RT)\ s^{-1}$, where R is expressed in units of cal/(K mol).

As has been mentioned before, phenylnitrene (which is being analyzed experimentally as aniline) and cyclopentadiene carbonitrile, together with carbon monoxide, are the major products of the thermal decomposition of anthranil; their mole percents together are close to 100%. Their formation can be expressed by the following general schematic pathways:

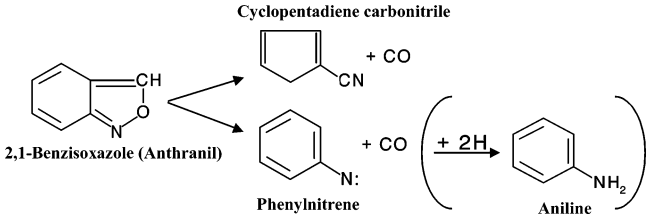

This is a complex set of unimolecular reactions and the purpose of this investigation is to determine the detailed mechanism of their formation by quantum chemical calculations and to compare the results of the calculations with the experimental, single pulse shock tube results.

III. Quantum Chemical Calculations

1. Calculation of the Critical Points on the Adiabatic Potential Energy Surfaces (PES). Geometry optimization of the reactant, products, intermediates and transition states on both the singlet and the triplet potential energy surfaces were carried out at the Becke three-parameter hybrid method[13] with Lee−Yang−Parr correlation functional approximation with unrestricted open shell wave functions (uB3LYP).[14] The Dunning correlation consistent polarized valence double ξ (cc-pVDZ) basis set[15] was used. For determining transition-state structures, we used the combined synchronous transit-guided quasi-Newton (STQN) method.[16]

All the calculations were performed without symmetry restrictions. Vibrational analyses were done at the same level of theory to characterize the optimized structures as local minima or transition states. Calculated vibrational frequencies and entropies (at the uB3LYP level) were used to evaluate preexponential factors of the reactions under consideration. All the calculated frequencies, the zero point energies and the thermal energies are of harmonic oscillators. The calculations of the intrinsic reaction coordinate (IRC), to check whether the transition states under consideration connect the expected reactants and products, were done at the uB3LYP level of theory with the same basis set as was used for the stationary point optimization. We verified also that each transition state has one imaginary frequency

Each optimized uB3LYP structure was recalculated at a single-point using quadratic CI including single and double substitutions with a triple contribution to the energy, uQCISD-(T).[17] All of the reported relative energies include zero-point energy (ZPE) correction.

2. Location of the Crossing Points between the Singlet and the Triplet PES and Estimation of the Crossing Probability. We used the gradient-based method to find the minimum energy crossing point (MECP) between the singlet and triplet surfaces (i.e., the lowest points with the same geometry, where the two states have the same energy). The algorithm involves an energy minimization on one surface under the constraint that the two surfaces will have the same energy.[18,19] This algorithm was used to calculate the energies and the gradients on both surfaces. We used for this procedure the same combination of method/basis set, namely, uB3LYP/cc-pVDZ.

To calculate the spin−orbit coupling (SOC) at the minimum energy crossing points, the one- and two-electron full Pauli−Breit operator method was used.[20] The wave functions for the SOC were optimized with the complete active space self-consistent field theory (CASSCF) in the region of the MECP that was found by using the B3LYP method. The active space of the wave functions consisted of 12 electrons distributed in 10 orbitals, CASSCF(12,10), including the π system of the two rings (six- and five-membered), p-orbitals of the nitrogen and oxygen atoms and one σ N−O bond that is being broken. For species without the CO group, an active space of 10 electrons and 8 orbitals was used, CASSCF(10,8). These multiconfiguration wave function calculations used the same basis set as uB3LYP calculations.

The multiple passage crossing probability at the MECP can be estimated with the semiclassical Landau−Zener (LZ) approximation.[21,22] This probability depends on the spin−orbit coupling (SOC) and on the local topology of the PES (through the energy difference gradient):

$$P_{LZ} = [1 - \exp(-2\pi\gamma)]/[1 - 0.5 \exp(-2\pi\gamma)]$$

where $\gamma = 2\pi^2\ (SOC)^2/h\upsilon\Delta F$. υ is the effective velocity of passing through the crossing point, and ΔF is the difference in the slopes of the two crossing potential curves in the direction orthogonal to the intersection seam at the MECP. The effective velocity was approximated by the average velocity in a one-dimensional Maxwell−Boltzmann distribution,[23]

$$\upsilon = (k_B T/2\pi\mu)^{1/2}$$

where μ is the reduced mass of the movement along the reaction coordinate.

It should be mentioned that this procedure is a qualitative estimate of the crossing probability of spin-forbidden reactions.[24−26]

The DFT and QCISD(T) computations were carried out using the Gaussian-03 program package[27] and the CASSCF and SOC calculations were carried out using the GAMESS-USA pro-

TABLE 1: Zero Point Energies, Imaginary Frequencies,[a] Entropies,[b] Spin Contaminations and Relative Energies ΔE^c of the Species on the Singlet Surfaces

species	uB3LYP ZPE	S^b	$\langle S^2\rangle$	ν^a	uQCSID(T) ΔE^c
Pathway (S,α)					
anthranil	65.8	77.79			0.0
TS1(S)	62.2	82.68	1.0349	(i-172)	35.6
INT1(S)	63.0	84.34	1.0358		27.7
TS2(S,α)	60.8	86.09	0.0	(i-452)	62.0
INT2(S,α)	63.2	87.42	0.0		−9.1
TS3(S,α)	60.8	85.83	0.0	(i-1182)	18.0
INT3(S,α)	62.9	88.26	0.0		−10.0
TS4(S,α)	62.1	84.03	0.0	(i-419)	9.0
INT4(S,α)	62.9	87.45	0.0		−5.9
TS5(S,α)	58.5	88.16	0.0	(i-978)	15.4
CPDN[d] + CO	60.4	123.83	0.0		−14.4
Pathway (S,β) Part I					
anthranil	65.8	77.79			0.0
TS1(S)	62.2	82.68	1.0349	(i-172)	35.6
INT1(S)	63.0	84.34	1.0358		27.7
TS2(S,β)	60.1	82.18	0.7597	(i-1319)	41.4
INT2(S,β) (CHKI)	64.3	85.26	0.0		−3.6
TS3(S,β)	60.4	93.42	1.0322	(i-87)	49.1
phenylimine(S) + CO	59.9	121.41	1.0286		42.4
Pathway (S,β) Part II[e]					
phenylimine(S)	56.7	74.18	1.0286		0.0
TS4(S,β)	54.7	74.71	0.1190	(i-1189)	22.8
6-iminofulvene	56.9	76.37	0.0		−38.2
TS5(S,β)	53.1	78.47	0.0	(i-1039)	17.6
CPDN[d]	57.2	76.60	0.0		−56.8
TS6(S,β)	53.6	74.50	1.0329	(i-2190)	35.7
phenylnitrene(S)	57.1	79.96	1.0350		−19.1
TS7(S,β)	54.8	75.34	0.0	(i-548)	19.0
TS8(S,β)	54.9	75.15	0.0	(i-1216)	−30.9
CPDN[f]	57.2	76.35	0.0		−62.7
TS9(S,β)	53.4	80.62	1.0336	(i-307)	27.7
INT3(S,β)	53.6	85.33	1.0266		19.9
TS8(S,β)	53.3	79.45	0.6027	(i-259)	23.1

[a] Imaginary frequencies in cm^{-1}. [b] Entropies at 298 K in cal/(K mol). [c] Relative energies in kcal/mol. $\Delta E = \Delta E_{total} + \Delta(ZPE)$. [d] 1,3-Cyclopentadiene-5-carbonitrile. [e] Energies are relative to the energy of phenylimine(S) that is taken as zero. [f] 1,3-Cyclopentadiene-1-carbonitrile.

gram,[28] version December 2003. All the calculations were done on a DEC Alpha XP1000 1/667 professional workstation.

IV. Rate Constant Calculations

High-pressure limit first-order rate constants were evaluated from the results of the quantum chemical calculations using the relation:[29,30]

$$k_\infty = \sigma(k_B T/h)\exp(\Delta S^{\#}/R)\exp(-\Delta H^{\#}/RT)$$

where h is Planck's constant, k_B is the Boltzmann factor, σ is the degeneracy of the reaction coordinate, $\Delta H^{\#}$ and $\Delta S^{\#}$ are the temperature-dependent enthalpy and entropy of activation, respectively. Since we deal with unimolecular reactions, $\Delta H^{\#} = \Delta E^{\#}$, where $\Delta E^{\#}$ is the energy difference between the transition state and the reactant. $\Delta E^{\#}$ is equal to $\Delta E^0_{total} + \Delta E_{thermal}$, where ΔE^0_{total} is obtained by taking the difference between the total energies of the transition state and the reactant and $\Delta E_{thermal}$ is the difference between the thermal energies of these two species.

The rate constant for spin-crossing processes was calculated from the relation

$$k_\infty = P_{LZ}\sigma(k_B T/h)\exp(\Delta S_{cr}/R)\exp(-\Delta E_{cr}/RT)$$

TABLE 2: Arrhenius Parameters of the Elementary Steps on the Singlet and Triplet PES Including the S → T and T → S Intersystem Crossing Rate Constants

		A^a	$E_a{}^b$
Pathways on the Singlet PES (Figures 5 and 6)			
1	anthranil(S) → INT1(S)	6.11×10^{14}	37.86
2	INT1(S) → INT2(S,α) (1,3-cyclopentadiene-5-carbonitrile + CO)	1.06×10^{14}	36.00
3	INT1(S)→ INT2(S,β) (CHKI)	9.90×10^{12}	14.51
4	INT2(S,β) (CHKI) → phenylimine(S) + CO	3.14×10^{15}	55.14
5	phenylimine(S) → 6-iminofulvene	4.68×10^{13}	24.10
6	6-iminofulvene → 1,3-cyclopentadiene-5-carbonitrile	1.29×10^{14}	57.61
7	phenylimine(S) → phenylnitrene(S)	3.17×10^{13}	36.79
8	phenylnitrene(S) → 1,3-cyclopentadiene-5-carbonitrile	9.73×10^{13}	39.89
9	1,3-cyclopentadiene-5-carbonitrile → 1,3-cyclopentadiene-1-carbonitrile	1.22×10^{14}	26.62
Pathways on the Triplet PES Including the S → T and T → S Crossings (Figures 9 and 10)			
10[c]	anthranil(S) → INT1(T)	5.88×10^{14}	38.48
11	INT1(T)→ INT2(T)	8.93×10^{12}	6.16
12	INT2(T) → INT3(T)	1.19×10^{13}	21.13
13	INT3(T) → phenylimine(T) +CO	3.46×10^{15}	20.46
14	phenylimine(T) → phenylnitrene(T)	1.81×10^{13}	32.91
15[c]	phenylnitrene(T) → phenylnitrene(S)	1.26×10^{11}	22.93
16	phenylnitrene(T) → INT4(T)	4.50×10^{15}	47.90
17[c]	INT4(T) → INT5(S)	1.20×10^{9}	5.98
18	INT5(S) → 1,3-cyclopentadiene-5-carbonitrile	9.46×10^{11}	3.34

[a] Preexponential factor in units of s^{-1}. [b] Activation energy in kcal/mol. [c] Crossing steps.

TABLE 3: Zero Point Energies, Imaginary Frequencies,[a] Entropies,[b] and Relative Energies ΔE^c of the Species on the Triplet Potential Energy Surface and of the Crossing Points

species	uB3LYP ZPE	S^b	ν^a	uQCSID(T) ΔE^c
Pathway (T) Part I[d]				
anthranil(S)	65.8	77.79		0.0
anthranil(T)	62.9	81.93		50.3
TS1(T)	62.0	82.06	(i-1049)	62.3
MECP1	63.6	82.33(S)		35.4
		85.07(T)		
INT1(T)	63.0	86.17		21.6
TS2(T)	62.3	84.56	(i-160)	27.2
INT2(T)	63.1	86.25		19.6
TS3(T)	60.2	84.33	(i-1805)	39.8
INT3(T)	63.3	84.34		22.1
TS4(T)	60.6	95.02	(i-101)	40.4
phenylimine(T) + CO	60.0	123.40		39.3
Pathway (T) Part II[e]				
phenylimine(T)	56.9	76.14		0.0
TS5(T)	54.0	75.45	(i-2110)	32.0
phenylnitrene(T)	57.2	75.90		−24.5
MECP2	55.5	72.48(S)		−2.4
		74.44(T)		
TS6 (T)	53.6	81.29	(i-275)	20.7
MECP3	53.2	81.92(S)		24.8
		84.81(T)		
INT4 (T)	53.8	86.90		19.1
TS7 (T)	53.2	80.60	(i-599)	38.9

[a] Imaginary frequencies in cm^{-1}. [b] Entropies at 298 K in cal/(K mol). [c] Relative energies in kcal/mol. $\Delta E = \Delta E_{total} + \Delta(ZPE)$. [d] Energies are relative to the energy of anthranil(S) that is taken as zero. [e] Energies are relative to the energy of phenylimine(T) that is taken as zero.

where P_{LZ} is the crossing probability and ΔS_{cr} and ΔE_{cr} are the difference between the entropy and the energy at the crossing point and the nearest local minimum (reactant or intermediate), respectively.

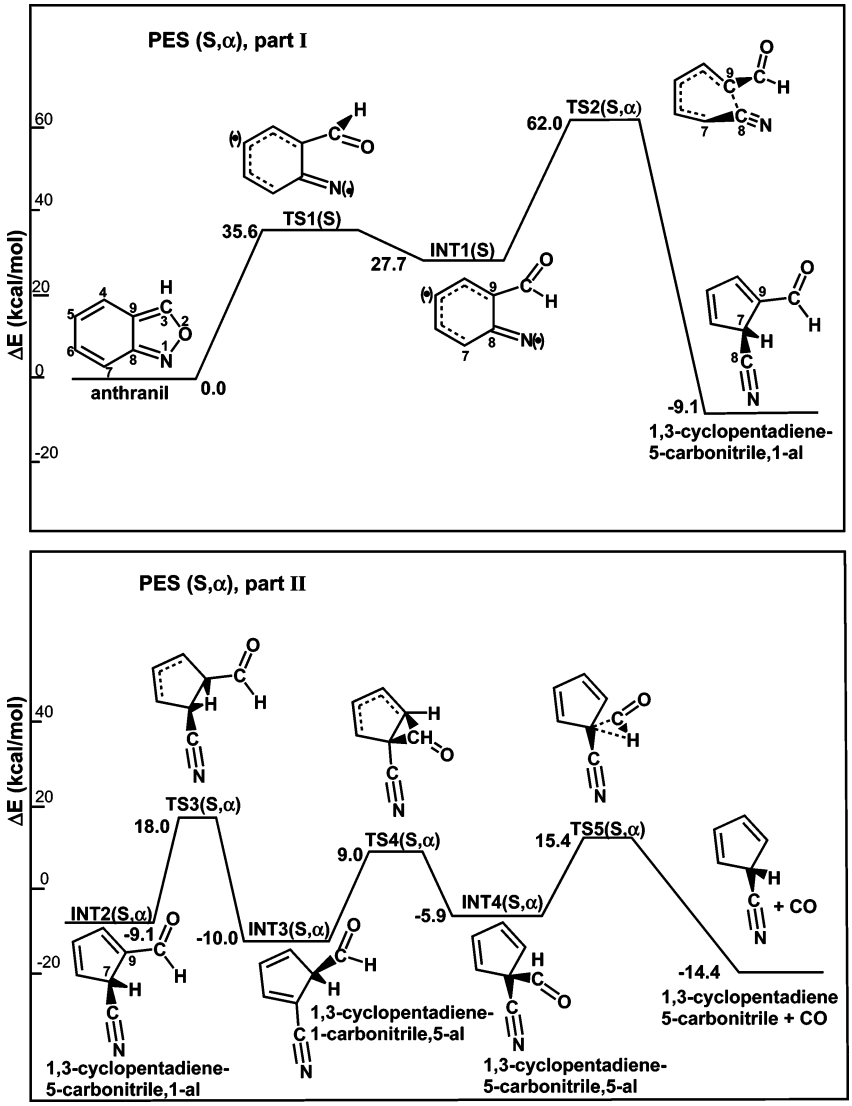

Figure 5. Reaction pathway of anthranil decomposition where ring contraction takes place following CO elimination. Relative energies (in kcal/mol) are calculated at the uQCISD(T)//uB3LYP/cc-pVDZ level of theory. (●) denotes partially distributed free electron density.

It should be mentioned that errors in the crossing probability (P_{LZ}) will have a rather small effect on the crossing rate as compared to errors in the location of MECP as the barrier (ΔE_{cr}) for the crossing point appears in the exponent whereas the crossing probability appears in the preexponential factor.

V. Discussion

1. Pathways on Singlet Potential Energy Surfaces. For cyclopentadiene carbonitrile to be formed from anthranil, two processes must take place. These are ring contraction of the six-membered ring to a five-membered ring and elimination of CO. These two processes can take place where CO is eliminated following (α) or prior to (*β*), ring contraction. The first step that is common to both processes is rupture of the weak N−O bond with a low barrier of ∼36 kcal/mol at uQCISD(T)//uB3LYP/cc-pVDZ level of theory. The bond energy is particularly low since the six-membered ring in anthranil has no resonance stabilization. Moreover, some resonance is formed in the transition state (TS1(S)), Figure 5, I. Following a rotation of the HCO group and some additional resonance stabilization, an intermediate INT1(S) that is again common to the two processes (Figure 5, I) is formed, at an energy level of 27.7 kcal/mol above that of anthranil.

a. CO Elimination Following Ring Contraction (α). Parts I and II of Figure 5 show the potential energy surface (PES(S,α)) where ring contraction occurs prior to CO elimination. For ring contraction to take place, C(8)−C(9) has to be broken. The corresponding transition state TS2(S,α) is at an energy level of 62 kcal/mol. Following several steps that involve the migration of the HCO group from C(9) to C(7) together with H-atom shift from C(7) to C(9) and CO elimination cyclopentadiene carbonitrile is formed. It should be mentioned that the CO elimination proceeds with a higher barrier when the HCO group is attached to C(9) as the C(9)−CHO bond energy is higher than that of the C(7)−CHO bond. This can be seen by the large C(7)−CHO bond distance (1.57 Å) as compared to the lower C(9)−CHO one (1.53 Å). This is the reason for the many steps that can be seen on the surface PES(S,α) in Figure 5, II.

b. CO Elimination Prior to Ring Contraction (β). Parts I and II of Figure 6 show the potential energy surface (PES(S,*β*)) where CO elimination occurs prior to ring contraction. The reaction coordinate in the transition state TS2(S,*β*) is 1,4-H atom migration from C(3) to N(1) with the formation of *o*-cyclohexadienylidene keteneimine (CHKI). The thermochemistry shows that at equilibrium the ratio *o*-cyclohexadienylidene keteneimine to anthranil is ∼325 at 900 K. Also, in view of

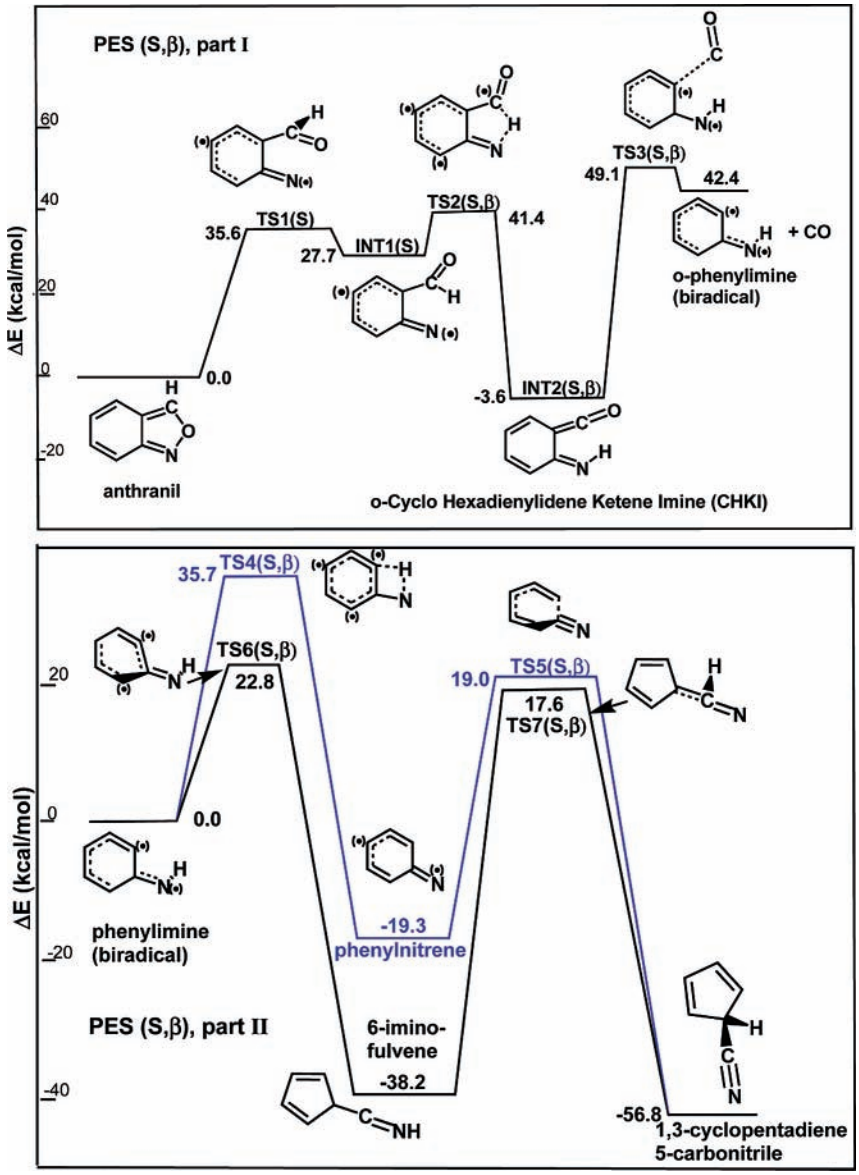

Figure 6. Reaction pathway of anthranil decomposition where CO elimination takes place prior ring contraction. Relative energies (in kcal/mol) are calculated at the uQCISD(T)//uB3LYP/cc-pVDZ level of theory. (●) denotes partially distributed free electron density.

the low barrier, equilibrium is attained at the very early stages of the reaction. This means that on PES(S,β) the process is practically determined by the reactions of CHKI. With a barrier of 52.7 kcal/mol and $\Delta S^{\#}$ of some 8 cal/(K•mol) CO is eliminated with the formation of *o*-phenylimine (biradical).

By examining the two potential energy surfaces (α) and (β), we can see that the intermediate INT1(S) that is formed in the first step on both surfaces can proceed via two parallel reactions. However, the barrier on surface (α) to reach the first transition state TS2(S,α) namely, 34.3 kcal/mol (Figure 5, I) is much higher than the one on surface (β), which is only 13.7 kcal/mol (Figure 6, I). This means that INT1(S) will be almost completely channeled to the intermediate INT2(S,β) via transition state TS2-(S,β). It can therefore be concluded that the potential energy surface (α) does not contribute to the decomposition of anthranil, and thus CO elimination occurs only prior to ring contraction.

o-Phenylimine that is formed following CO elimination (Figure 6, I), further isomerizes to two isomerization products (Figure 6, II). One involves an H-atom migration to form phenylnitrene, and in the second one the six-membered ring is contracted to a five-membered ring forming 6-iminofulvene. Since, however, the barrier for the formation 6-iminofulvene is ~13 kcal/mol lower than the one for the formation of phenylnitrene (Figure 6, II), the latter is practically the only product of the isomerization with only a very small leakage to phenylnitrene.

As has been shown previously, aniline is a major product in the postshock samples of anthranil decomposition. It can be obtained by a reaction of phenylimine or phenylnitrene with traces of water that are absorbed on the injection system of the gas chromatograph, on the column or elsewhere. Aniline cannot be produced by a reaction of 6-iminofulvene with traces of absorbed water. On the other hand, phenylimine isomerizes very rapidly to 6-iminofulvene. The question that arises is whether the small quantities of either phenylimine or phenylnitrene are high enough to account for the observed high concentration of aniline. Also, the question is to what extent 6-iminofulvene can overcome the high barriers on both sides and produce enough 1,3-cyclopentadiene-5-carbonitrile. To answer these two questions, we have carried out multiwell calculations to determine an overall rate constant and production rates of the main decomposition products, and to compare the calculations to the single pulse shock-tube results.

2. Multiwell Calculations and Kinetic Modeling on the Singlet Potential Energy Surface. It should be mentioned that

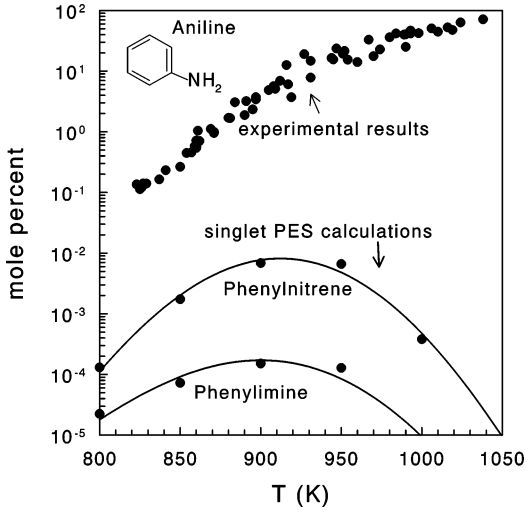

Figure 7. Plots of the calculated mole percent of phenylnitrene and phenylimine, the precursors of aniline, on the singlet PES. The experimental data points are shown for comparison. The very low mole percent of phenylnitrene and phenylimine cannot account for the large mole percent of the aniline.

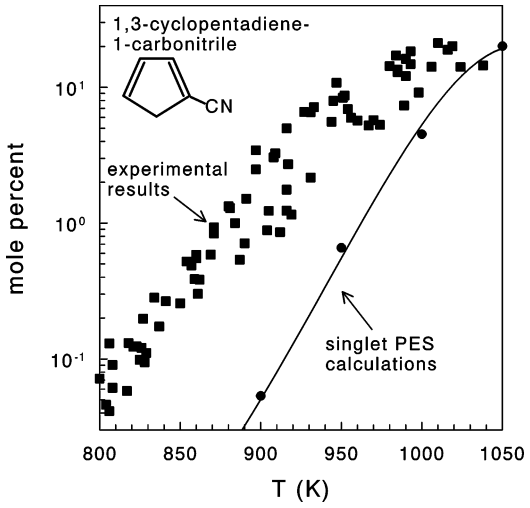

Figure 8. Plots of the calculated mole percent of 1,3-cyclopentadiene-1-carbonitrile on the singlet PES. The experimental data are shown for comparison. The agreement is very poor.

in order to evaluate an equivalent rate constant for a given reaction that is composed of several elementary steps, a kinetic scheme has to be constructed, including both the forward and the back reactions, and computer simulation has to be carried out. For this purpose the rate constants of the elementary steps on the surface were calculated at several temperatures as previously described, covering the temperature range at which the single pulse shock-tube experiments were carried out. These were then plotted as ln k vs. $1/T$ to obtain Arrhenius type rate constants. The unimolecular rate constants that were calculated on the potential energy surfaces, namely k_∞, were used in the reaction scheme without RRKM corrections since the temperatures were rather low and the species under consideration are large. These rate constants together with the calculated thermodynamic properties of the species involved (reactant, intermediates and products) were introduced into the kinetic scheme (Table 2), and the fraction of each intermediate and product was evaluated.

Figures 7 and 8 show a comparison between the experimental, single pulse shock-tube results and the results of the quantum chemical calculations. As can be seen in Figure 7, the calculated mole percent of phenylnitrene and phenylimine, the precursors of aniline, are orders of magnitude below the mole percent of the experimentally observed aniline and thus cannot account for its high concentration. Figure 8 shows a comparison between the calculated and the experimental mole percent of the sum of two isomers, 1,3-cyclopentadiene-5-carbonitrile and 1,3-cyclopentadiene-1-carbonitrile. Although 1,3-cyclopentadiene-5-carbonitrile is formed on the potential energy surface, it very rapidly, with a barrier of ~26 kcal/mol, interisomerizes to 1,3-cyclopentadiene-1-carbonitrile, as the latter is more stable by some 6 kcal/mol (TS8 in Table 1). Thus, 1,3-cyclopentadiene-1-carbonitrile is the isomer that is found in the postshock mixtures and is used for comparison between the experimental and calculated values. As can be seen in Figure 8, the calculated values are orders of magnitude below the experimental ones, particularly at the low-temperature end.

The computer modeling shows that, because of high barriers from both sides of 6-iminofulvene, the latter has the highest concentration among the various intermediates and products. Nevertheless, we could not identify any fulveneimine in the postshock samples.

In view of these two discrepancies between the experimental results and quantum chemical calculations, namely, the unexplained very low mole percent of cyanocyclopentadiene carbonitrile and of the precursors of aniline, we tried to search for additional pathways on singlet surfaces that will be compatible with the experimental results. As these could not be found, we decided to examine the possibility that the reaction proceeds on a triplet surface.

3. Pathways on a Triplet Potential Energy Surface. Figure 9, I is the first part of a triplet potential energy surface with a pathway that leads to the formation of a triplet *o*-phenylimine. In contrast to the singlet surfaces where there are two reaction pathways, namely, CO elimination prior to and following ring contraction, we could find only one reaction pathway on a triplet surface, and on this surface CO elimination occurs prior to ring contraction. The triplet surface has an additional intermediate INT1(T), but all the others species are similar to those on the singlet surface that have open shell.

The initial singlet → triplet crossing point was found to be at a level of 35.4 kcal/mol above the ground-state energy of the singlet anthranil (Figure 9, I) and it is below the energy level of the transition state TS1(S) on the singlet potential energy surface. The crossing point (MECP1), the spin−orbit coupling (SOC), ΔF, μ and the singlet → triplet crossing probability (P_{LZ}) were calculated as described in section III.2. The value of P_{LZ} was 0.03 at $T = 900$ K, where SOC = 47 cm^{-1}, $\Delta F = 3.7$ ev/Å and $\mu = 11.5$ amu.

The main difference between the pathways on the triplet and on the singlet surfaces can very well be seen by comparing Figure 9, II, with Figure 6, II. In Figure 9, II, there is only one isomerization product of the triplet phenylimine which is phenylnitrene and it can lead to the formation of aniline. In Figure 6, II, singlet phenylnitrene, on the other hand is formed, but with a high barrier (35.7 kcal/mol), so that the latter cannot compete with the low barrier for the formation of 6-iminofulvene (22.8 kcal/mol) and thus cannot account for the experimentally observed aniline.

It has been shown that triplet phenylnitrene dimerizes to azobenzene, whereas singlet phenylnitrene produces cyclopentadiene carbonitrile.[31] This means that the pathway that leads to the formation of triplet 1,3-cyclopentadiene-5-carbonitrile from triplet phenylnitrene as shown in Figure 9, II is to some extent unreal. Moreover, the barrier of its formation, 63.4 kcal/mol, is very high. We therefore looked for crossing point from

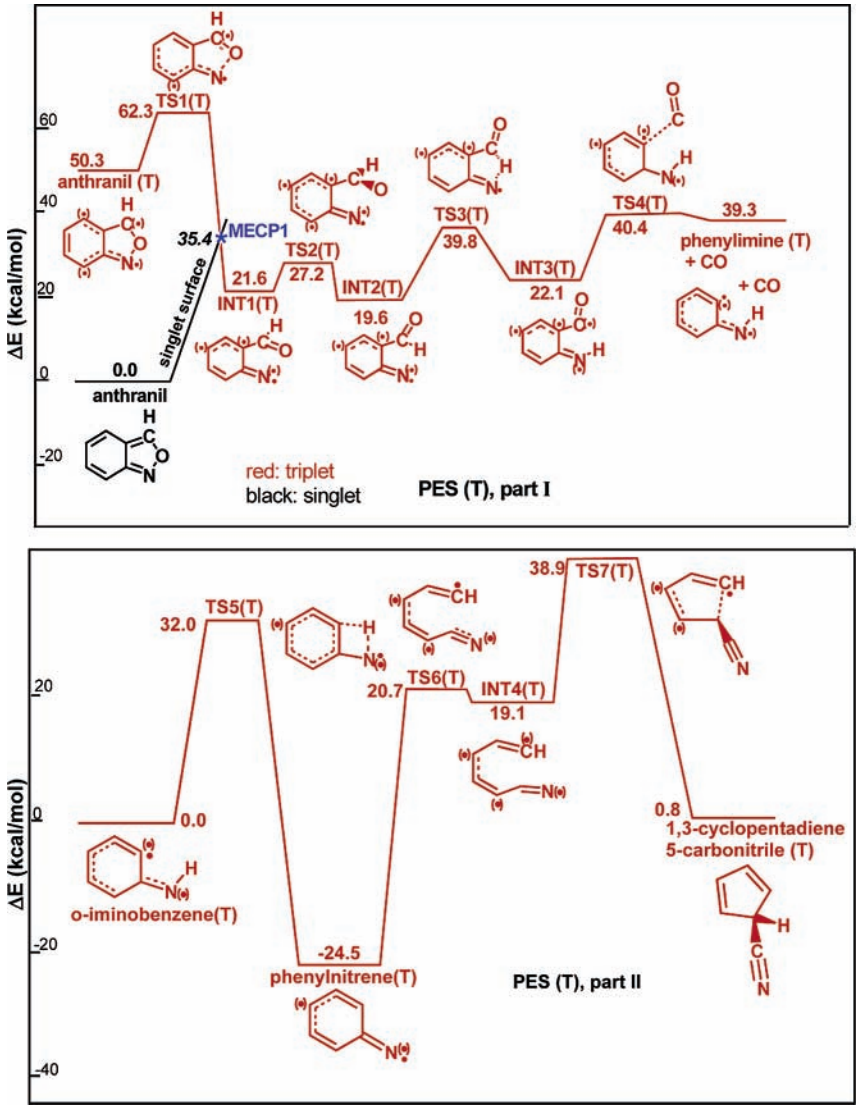

Figure 9. Reaction pathway of anthranil decomposition on the triplet potential energy surface. Relative energies (in kcal/mol) are calculated at uQCISD(T)//uB3LYP/cc-pVDZ level of theory. (●) denotes partially distributed free electron density.

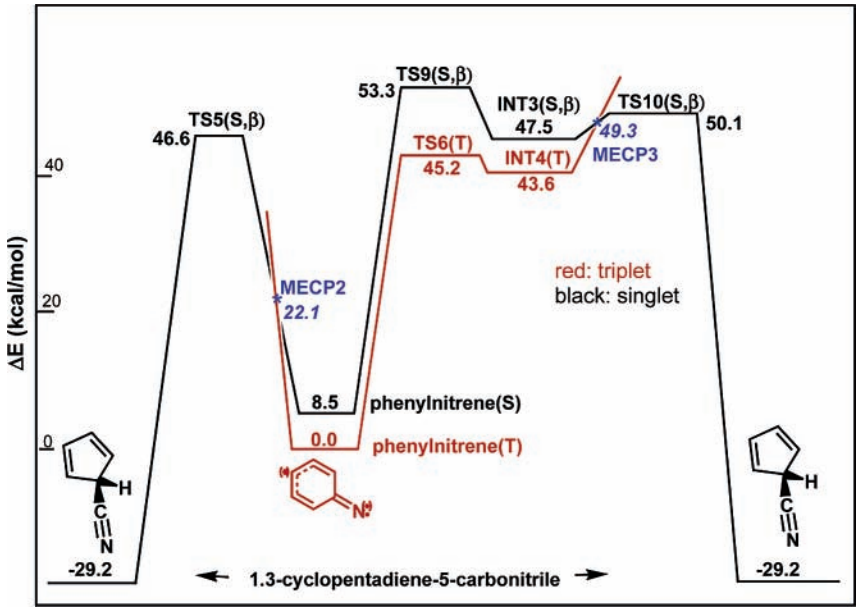

Figure 10. Reaction pathway for the formation of singlet 1,3-cyclopentadiene-5-carbonitrile from triplet phenylnitrene. The two triplet → singlet MECP are shown at the two sides of triplet phenylnitrene. MECP2 is the main contributor to the formation of 1,3-cyclopentadiene-5-carbonitrile. Relative energies (in kcal/mol) are calculated at uQCISD(T)//uB3LYP/cc-pVDZ level of theory. (●) denotes partially distributed free electron density.

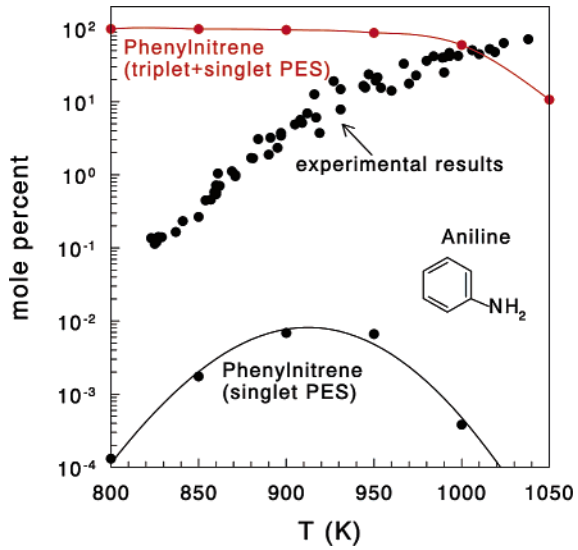

Figure 11. Plots of the calculated mole percent of phenylnitrene, the precursor of aniline, on the triplet PES. The experimental data points and the calculated points on the singlet surface are shown for comparison. The very high mole percent of phenylnitrene can easily account for the large mole percent of the aniline.

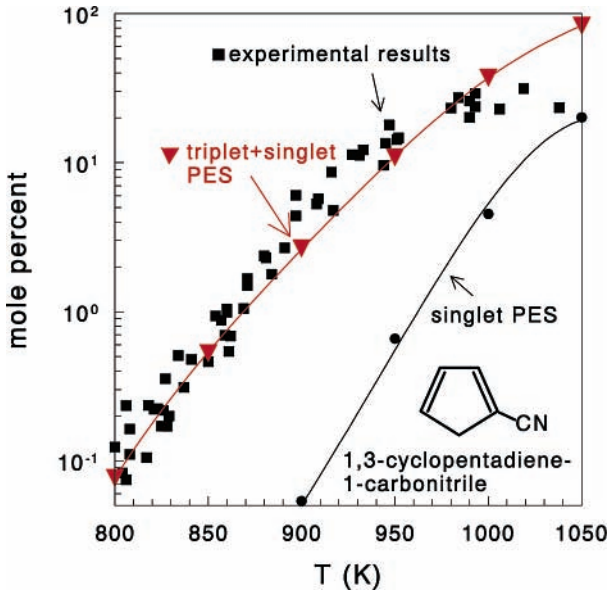

Figure 12. Plots of the calculated mole percent of 1,3-cyclopentadiene-1-carbonitrile on the triplet surface. The experimental data points (blue squares) are in reasonably good agreement with the calculated points (red filled circles). The calculation included all the elementary steps on both the singlet and the triplet surfaces. The results of 1,3-cyclopentadiene-1-carbonitrile formation on the singlet PES only are shown for comparison.

the triplet to the singlet phenylnitrene. We did find two crossing points at energies of 22.1 and 49.3 kcal/mol with respect to the level of phenylnitrene triplet. The two crossing points MECP2 and MECP3 are shown in Figure 10, drawn at the two sides of phenylnitrene(T). The values of P_{LZ} were 0.007 for MECP2 and 0.003 for MECP3 at $T = 900$ K, where SOC = 7 and 4 cm^{-1}, respectively. The crossing rate constants are shown in Table 2, part II.

Note that triplet phenylnitrene is the ground state of this molecule and is thus more stable than the singlet.[32−40] According to our calculations the difference is 8.5 kcal/mol.

4. Multiwell Calculations and Kinetic Modeling on the Triplet Potential Energy Surface. Table 2, part II, shows the kinetic scheme for the reactions of all the species on the triplet potential energy surface including the singlet → triplet and the triplet → singlet crossing rate constants. The modeling was performed as has been described in the section V.2 on the multiwell calculations of the singlet surfaces, where both the forward and the back reactions were taken in the account. It includes also all the species of the reactions on the singlet surfaces as they take place in parallel to the triplet surface reactions. The results of the calculations in terms of mole percent are shown in Figures 11 and Figure 12 for aniline and cyclopentadiene carbonitrile in comparison to experimental results. As can be seen (Figure 11), the mole percent of the triplet phenylnitrene is very high and can easily account for the large mol percent of aniline that was found experimentally. The mol percents of phenylnitrene and phenylimine that were calculated on the singlet surface are also shown for comparison. Figure 12 shows the results for 1,3-cyclopentadiene-1-carbonitrile. As can be seen, the agreement is quite satisfactory.

VI. Conclusions

(a) Two singlet potential energy surfaces that were found and analyzed could not account for the experimentally observed concentrations of cyclopentadiene carbonitrile and aniline that are the main decomposition products of anthranil. No other singlet potential energy surfaces that lead to the formation of the above two decomposition products could be found.

(b) In view of conclusion discussed in (a) the possibility that the reaction proceeds on a triplet potential energy surface was explored. A triplet surface where CO is eliminated prior to ring contraction and that leads to the formation of cyclopentadiene carbonitrile and phenylnitrene was found. Singlet → triplet and triplet → singlet crossing points were found, and crossing probabilities were calculated. Multiwell calculations on the triplet surface (including also the pathways on the singlet surface) reproduced very well the mole percent of cyclopentadiene carbonitrile and could account for the high mole percent of aniline.

(c) Although the two singlet potential energy surfaces look quite reasonable, they were ruled out as channels for production of the main decomposition products of anthranil only on the basis of being incompatible with the experimental results. An important conclusion, therefore, is that if the results of a calculated potential energy surface cannot be anchored to some existing experimental results, then the surfaces should be viewed with some skepticism.

Acknowledgment. This work was supported by the ISF, The Israel Science Foundation under grant agreement # 34/01. We thank Dr. Shmuel Zilberg and Mr. Semyon Cogan for very helpful discussions.

References and Notes

(1) Steele, W. V.; Chirico, R. D.; Knipmeyer, S. E.; Nguyen, A. *J. Chem. Thermodyn.* **1992**, *24*, 449.
(2) Matos, M. A.; Miranda, M. S.; Morais, V. M. F.; Liebman, J. F. *Eur. J. Org. Chem.* **2004**, 3340.
(3) Lifshitz, A.; Wohlfeiler, D. *J. Phys. Chem.* **1992**, *96*, 4505.
(4) Lifshitz, A.; Wohlfeiler, D. *J. Phys. Chem.* **1992**, *96*, 7367.
(5) Lifshitz, A.; Wohlfeiler, D.; Tamburu, C. *J. Phys. Chem.* **1995**, *99*, 11436.
(6) Eswaran, S. V. *Chem. Heterocycl. Compds.* **1999**, *49*, 123.
(7) He, Y. Z.; Cui, J. P.; Mallard, W. G.; Tsang, W. *J. Am. Chem. Soc.* **1988**, *110*, 3754.
(8) Sakaizumi, T.; Kikuchi, H.; Ohashi, O.; Yamaguchi, I. *Bull. Chem. Soc. Jpn.* **1987**, *60*, 3903.
(9) Thetaz, C.; Crow, W. D. *J. Am. Chem. Soc.* **1976**, *98*, 1258.

(10) Wentrup, C.; Mayor, C.; Gleiter, R. *Helv. Chim. Acta* **1972**, *55*, 2628.
(11) Lifshitz, A.; Laskin, A. *J. Chem. Phys.* **1997**, *101*, 7787.
(12) Westly, F.; Herron, J. T.; Cvetanovic, R. J.; Hampson, R. F.; Mallard, W. G. *NIST − Chemical Kinetics Standard Reference Database 17*, Version5.0; Nataional Institute of Standards and Technology: Washington, DC, 1998.
(13) Becke, A. D. *J. Chem. Phys.* **1993**, *98*, 5648.
(14) Lee, C.; Yang, W.; Parr, R. G. *Phys. Rev.* **1988**, *B37*, 785.
(15) Dunning, T. H., Jr. *J. Chem. Phys.* **1989**, *90*, 107.
(16) Peng, C.; Schlegel, H. B. *Isr. J. Chem.* **1993**, *33*, 449.
(17) Pople, J. A.; Head-Gordon, M.; Raghavachari, K. J. *J. Chem Phys.* **1987**, *87*, 5968.
(18) Harvey, J. N.; Aschi, M.; Schwarz, H.; Koch, W. *Theor. Chem. Acc*. **1998**, *99*, 95.
(19) Poli, R.; Harvey, J. N. *Chem. Soc. Rev.* **2003**, *32*, 1.
(20) Fedorov, D.; Koseki, S.; Schmidt, M. W.; Gordon, M. S. *Int. Revi. Phys. Chem.* **2003**, *22*, 551.
(21) Nakamura, H.; Zhu, C. *Comments At. Mol. Phys.* **1996**, *32*, 249.
(22) Kuznetsov, A. M. *Stochastic and Dynamic views of chemical reaction kinetics in solutions*; Presses polytechiques et universitaires romandes: CH-1015 Lausanne, 1999.
(23) Hess, J. S.; Doren, D. J. *J. Phys. Chem. B* **2002**, *106*, 8206.
(24) Harvey, J.; Aschi, M. *Faraday Discuss.* **2003**, *124*, 129
(25) German, E. D.; Efremenko, I.; Sheintuch, M. *J. Phys. Chem. A* **2001**, *105*, 11312.
(26) Arenas, J. F.; Marcos, J. I.; Lopez-Tocon, I.; Otero, J. C.; Soto, J. *J. Chem. Phys.* **2000**, *113*, 2282.
(27) Frisch, M. J.; Trucks, G. W.; Schlegel, H. B.; Scuseria, G. E.; Robb, M. A.; Cheeseman, J. R.; Montgomery, J. A., Jr.; Vreven, T.; Kudin, K. N.; Burant, J. C.; Millam, J. M.; Iyengar, S. S.; Tomasi, J.; Barone, V.; Mennucci, B.; Cossi, M.; Scalmani, G.; Rega, N.; Petersson, G. A.; Nakatsuji, H.; Hada, M.; Ehara, M.; Toyota, K.; Fukuda, R.; Hasegawa, J.; Ishida, M.; Nakajima, T.; Honda, Y.; Kitao, O.; Nakai, H.; Klene, M.; Li, X.; Knox, J. E.; Hratchian, H. P.; Cross, J. B.; Bakken, V.; Adamo, C.; Jaramillo, J.; Gomperts, R.; Stratmann, R. E.; Yazyev, O.; Austin, A. J.; Cammi, R.; Pomelli, C.; Ochterski, J. W.; Ayala, P. Y.; Morokuma, K.; Voth, G. A.; Salvador, P.; Dannenberg, J. J.; Zakrzewski, V. G.; Dapprich, S.; Daniels, A. D.; Strain, M. C.; Farkas, O.; Malick, D. K.; Rabuck, A. D.; Raghavachari, K.; Foresman, J. B.; Ortiz, J. V.; Cui, Q.; Baboul, A. G.; Clifford, S.; Cioslowski, J.; Stefanov, B. B.; Liu, G.; Liashenko, A.; Piskorz, P.; Komaromi, I.; Martin, R. L.; Fox, D. J.; Keith, T.; Al-Laham, M. A.; Peng, C. Y.; Nanayakkara, A.; Challacombe, M.; Gill, P. M. W.; Johnson, B.; Chen, W.; Wong, M. W.; Gonzalez, C.; Pople, J. A. *Gaussian 03*, revision B.05; Gaussian, Inc.: Wallingford, CT, 2003.
(28) Schmidt, M. W.; Baldrige, K. K.; Boatz, J. K.; Elbert, S. T.; Gordon, M. S.; Jensen, J. H.; Koseki, S.; Matsunaga, J. A.; Nguyen, K. A.; Su, S. J.; Windus, T. L.; Dipuis, M.; Montgomery, J. A. *J. Comput. Chem.* **1993**, *14*, 1347.
(29) Eyring, H. *J. Chem Phys.* **1935**, *3*, 107.
(30) Evans, M. G.; Polanyi, M. *Trans. Faraday Soc.* **1935**, *31*, 875.
(31) Crow, W. D.; Paddon-Row: M. N.; Sutherland, D. S. *Tetrahedron Lett.* **1972**, 2239.
(32) Cristsan, N. P.; Platz, M. S. *Adv. Phys. Org. Chem.* **2001**, *36*, 255.
(33) Drzaic, P. S.; Brauman, J. I. *J. Am. Chem. Soc.* **1984**, *106*, 3443.
(34) Drzaic, P. S.; Brauman, J. I. *J. Phys. Chem.* **1984**, *88*, 5285.
(35) Ozawa, K.; Ishida, T.; Fuke, K.; Kaya, K. *Chem. Phys. Lett.* **1988**, *150*, 249.
(36) Galbraith, J. M.; Gaspar, P. P.; Borden, W. T. *J. Am. Chem. Soc.* **2002**, *124*, 11669.
(37) Smolinsky, G.; Wasserman, E.; Yager, W. A. *J. Am. Chem. Soc.* **1962**, *84*, 3220.
(38) Castell, O.; Garcia, V. M.; Bo, C.; Caballol, R. *J. Comput. Chem.* **1996**, *17*, 42.
(39) Kim, S.-J.; Hamilton, T. P.; Schaefer, H. F., III *J. Am. Chem. Soc.* **1992**, *114*, 5349.
(40) Hrovat, D. A.; Waali, E. E.; Borden, W. T. *J. Am. Chem. Soc.* **1992**, *114*, 8698.